RSC Advances

PAPER

View Article Online
View Journal | View Issue

Cite this: *RSC Adv.*, 2016, **6**, 66553

Highly water-resistant carbon nanotube supported $PdCl_2$–$CuCl_2$ catalysts for low temperature CO oxidation†

Fanyun Zhou,[a] Xuexun Du,[a] Jun Yu,*[a] Dongsen Mao[a] and Guanzhong Lu*[ab]

Received 12th June 2016
Accepted 28th June 2016

DOI: 10.1039/c6ra15205h

www.rsc.org/advances

Carbon nanotube (CNT) supported $PdCl_2$–$CuCl_2$ catalysts were prepared by the two-step impregnation method, and the effects of the Pd and Cu loadings on their physicochemical properties and catalytic performance for low-temperature CO oxidation in the presence of high concentration moisture were investigated. With the increase in the Pd and Cu loadings, the surface active Pd^{2+} and Cu^{2+} species increased, improving the adsorption of CO and oxygen, and the oxidation of Pd^0 to Pd^{2+} (or Pd^+). Compared with Cu species, increasing the Pd loading can effectively add catalytically active sites for CO oxidation. For the CO oxidation, the presence of moderate water is necessary for sustaining the high activity of this catalyst, but the excessive water vapor in the feed gas would injure the activity and stability of the catalyst. When the moisture level in the reactant gas was 3.1%, the CO conversion was still retained at around 93% after 60 h of the reaction at 25 °C over the 3.3 wt% Pd–6.6 wt% Cu/CNT catalyst, indicating that this catalyst has very good stability and water-resistance.

1. Introduction

Catalytic oxidation of CO is very important for reducing the damage caused by automobile exhausts, elimination of environmental pollution and for fuel cell and carbon monoxide gas sensors[1–4] CO oxidation is often used as the probe reaction in the catalysis research. For low temperature CO oxidation, the design and preparation of the highly efficient and stable catalysts are very crucial. Among reported various catalysts, noble metal (Au, Pt, Pd) catalysts exhibit excellent activity for CO oxidation at low temperature.[5–8] Nano-Au catalysts were studied widely in recent years, because of its high catalytic activity for low temperature CO oxidation even in the presence of moisture.[9,10] However, there are still many defects with gold-based catalysts such as halogen compounds causing a detrimental effect on their activity, the inevitable decrease of activity with prolonged reaction time and deactivation during storage caused by indoor lights.[11–13] Pt catalysts usually exhibit higher activities for the CO-PROX reaction in H_2-rich gas,[14,15] but the CO conversion on Pt catalysts decreased sharply if the reaction was performed in the absence of H_2, and the CO was completely converted above 423 K.[16–19] Among the metal oxide catalysts for CO oxidation, Co_3O_4 and the Hopcalite catalyst (Cu–Mn–O) also show prominent catalytic activity at low temperatures, but the Co_3O_4 catalyst would be totally deactivated after 14 h of reaction in 3–10 ppm H_2O at room temperature, and the $Cu_{20}Mn_{80}O_x$ catalyst was deactivated after several minutes in relative humidity of 84% at 25 °C.[20,21] In the composite catalysts of the noble metal and transition metal oxides, the heterogeneous Wacker-type (supported $PdCl_2$–$CuCl_2$) catalyst has been widely researched, because of its high catalytic activity and superior stability for low temperature CO oxidation, even when in the reactant (or raw material) gas that includes halogen compounds and moisture.[22,23] Formerly, the supported $PdCl_2$–$CuCl_2$ catalysts were often prepared by a conventional impregnation method, and exhibited a significantly less catalytic activity than nano-gold catalysts for CO oxidation. To improve its activity and thermal stability, we have developed the NH_3 coordination–impregnation method[24] and the two-step impregnation method in the organic solvent[25] for Pd–Cu–Cl_x/Al_2O_3 catalyst preparation, resulting in the improvement of its catalytic activity and stability for low-temperature CO oxidation under conditions containing mild moisture.

For the Wacker-type catalyst, the nature and structure of the carrier can also have a significant influence on its catalytic performance for CO oxidation. As the carrier of the Wacker-type catalyst, Al_2O_3,[26–28] activated carbon (AC),[29,30] attapulgite clay,[31] and palygorskite[32] were studied a lot. As far as we know, the carbon nanotube (CNT) has not been studied as the carrier of the Wacker-type catalyst. Recently, CNTs have become a popular support, due to its special physical and chemical properties. Dai *et al.*[33] reported a modified CNT supported Ag catalyst, and

[a]*Research Institute of Applied Catalysis, School of Chemical and Environmental Engineering, Shanghai Institute of Technology, Shanghai 201418, China. E-mail: gzhlu@ecust.edu.cn; yujun@sit.edu.cn; Fax: +86-21-64252923*

[b]*Key Laboratory for Advanced Materials and Research Institute of Industrial Catalysis, East China University of Science and Technology, Shanghai 200237, China*

† Electronic supplementary information (ESI) available. See DOI: 10.1039/c6ra15205h

using this Ag catalyst and ~95% CO conversion was obtained at 70 °C after 24 h of the reaction in the H_2 rich mixed feed gas. Zhang *et al.*[34] successfully synthesized CeO_2–CuO/CNT nanocomposites by a simple pyridine-thermal method, and this catalyst exhibited a high catalytic performance for the CO oxidation without moisture: CO was completely converted at 175 °C. Kuo *et al.*[35] reported that the F–Co_3O_4/CNT catalyst exhibited outstanding activity and durability for CO oxidation at 150 °C under moisture-rich conditions.

In this study, we explored that CNT was used as the support of Pd–Cu–Cl_x, which was loaded on CNT by the two-step impregnation method. The effects of the Pd and Cu loadings on the physicochemical properties and the catalytic performance of the Pd–Cu–Cl_x/CNT catalyst for low-temperature CO oxidation were investigated in detail. The effects of CO and moisture concentrations on the CO oxidation over the 3.3 wt% Pd–6.6 wt% Cu/CNT catalyst were tested too. The results showed that CNT supported Wacker-type catalysts are a highly efficient, stable and water-resistant catalyst for low temperature CO oxidation.

2. Experimental section

2.1. Materials

The multiwall CNT (8–15 nm of outer diameter, 3–5 nm of inner diameter and 3–12 μm in length) was purchased from Suzhou Hengqiu Graphene Technology Co., Ltd (China). The commercial wood based (WAC) and coal based (CAC) activated carbons were purchased from Liyang Niuniu Activated Carbon Co., Ltd (China). $CuCl_2$, ethanol and propylene oxide reagents were analytical grade (AG) and purchased from Sinopharm Chemical Reagent Co., Ltd. (China). $PdCl_2$ (AG) was purchased from Adamas Reagent Co., Ltd.

2.2. Catalyst preparation

The Pd–Cu–Cl_x/CNT catalysts were prepared by the two-step impregnation method.[25] Weighted $CuCl_2$ was dissolved in 10 mL solution of propylene oxide (PO), ethanol and H_2O (volume ratio of PO/ethanol/H_2O was 1/1/6), and this mixed solution turned to light green and became turbid after 30 min of stirring. Then, 1.0 g CNT was added into this solution and stirred until well mixed. After being aged for 24 h, the Cu/CNT sample was dried at 120 °C for 4 h and calcined at 200 °C for 4 h. Weighted $PdCl_2$ was dissolved in 8 mL of 0.1 M hydrochloric acid, and then Cu/CNT sample was impregnated in this $PdCl_2$ solution and dried under vacuum at room temperature for 12 h. The loadings of Pd and Cu were 0.9–6.6 wt% and 1.7–9.9 wt%, respectively.

The calcination temperature of Cu/CNT sample was determined by thermal gravimetric analysis (TGA). In the TG curve of Cu/CNT (Fig. S1†), weight loss occurred steeply at >250 °C, which means that the supported Cu samples should be calcined at <250 °C, thus we chose 200 °C as the calcination temperature of Cu/CNT sample.

The Pd–Cu–Cl_x/WAC and Pd–Cu–Cl_x/CAC catalysts were prepared by the same method as the Pd–Cu–Cl_x/CNT catalysts. The Pd/CNT sample was prepared by impregnating CNT in the solution of $PdCl_2$ and dried under vacuum at room temperature for 12 h.

2.3. Catalytic activity testing

The catalytic performance of the catalyst for CO oxidation was tested in a fixed-bed quartz U-tube reactor (Ø 5 mm). 200 mg catalyst (20–40 mesh) was loaded in the reactor with some quartz wool plugged in both sides of the catalyst. The reactant gas comprised 1500 ppm CO and air. The feed gas (50 mL min^{-1}) went through a water vapor saturator immersed in a water bath (0–40°C) and was then inputted into the reactor. When the temperature of water bath was controlled at 25 °C, the concentration of water vapor in the reactant gas was 3.1%. The weight hour space velocity (WHSV) was 15 000 mL g^{-1} h^{-1}. The CO concentration was measured after the catalytic methylation by an online gas chromatograph (GC 2060) equipped with an FID under steady-state conditions.

The CO conversion (X) was calculated by

$$X\,(\%) = (CO_{inlet} - CO_{outlet})/CO_{inlet} \times 100$$

where CO_{inlet} indicates the initial CO concentration in the reactant gas and CO_{outlet} means the concentration of CO in the outlet.

2.4. Catalyst characterization

The thermo-gravimetric analysis (TGA) of samples were performed on a SAT 449 F3 Jupiter (NETZSCH) thermal analyzer at a heating rate of 10 °C min^{-1} under a continuous flow of air. The *in situ* FT-IR spectra were obtained on a Nicolet 6700 FT-IR spectrometer equipped with a MCT detector, in which the spectral resolution was 4 cm^{-1} and scan number was 128 times. The background spectrum was collected for pure KBr in the N_2 atmosphere. The sample to be measured was ground with KBr and the FT-IR spectra were tested before and after pretreatment at 120 °C in N_2 for 2 h. The X-ray diffraction (XRD) patterns of samples were recorded on a PANalytical X'Pert Pro MRD X-ray diffractometer (Netherlands) with CuKα radiation (λ = 0.154056 nm) operated at 40 kV and 40 mA. The transmission electron microscopy (TEM) images were obtained on a JEOL 2100F electron microscope operated at 200 kV. The samples were suspended in ethanol and supported onto a holey carbon film on a Cu grid. The Pd and Cu loading in the sample was measured by inductively coupled plasma optic emission spectrometry (ICP-OES) on a Pe Optima 2100 DV, and after the sample was solved in the mixed solution of 4 mL nitric acid, 1 mL perchloric acid and 1 mL hydrogen peroxide, which was further heated for 4 h at 180 °C under a static condition in a Teflon-lined autoclave. A nitrogen adsorption–desorption isotherm was measured at −196 °C on a Micrometrics ASAP 2020 apparatus. The surface area was calculated by the Brunauer–Emmett–Teller (BET) method. The average pore diameter and pore volume were determined by the Barrett–Joyner–Halenda (BJH) method, on the basis of the desorption branch of the isotherm. The X-ray photoelectron spectroscopy (XPS)

spectra were obtained on a Thermo Scientific ESCALAB 250Xi, the number of scans was 10 times, and pass energy was 30 eV in high resolution spectra and 160 eV in survey spectra. All binding energies (BE) were determined with respect to the C 1s line (284.6 eV) originating from adventitious carbon.

Temperature-programmed desorption of CO adsorbed onto the sample (CO-TPD) were carried out in the conventional flow system equipped with a quartz microreactor and a quadruple mass spectrometer (QMS, Balzers OmniStar 200) as the detector. The catalyst (0.1 g) was pretreated at 300 °C in the He flow (50 mL min^{-1}) for 1 h and cooled to room temperature (RT). After pure CO (10 mL min^{-1}) was introduced through the catalyst bed at RT for 30 min, He (50 mL min^{-1}) instead of pure CO swept the catalyst bed for 3 h. Subsequently, the sample was heated in a flowing He stream (50 mL min^{-1}) up to 250 °C at a rate of 10 °C min^{-1} and a quadruple mass spectrometer was used to monitor the desorbed species. The mass signals of CO ($m/z = 28$) and CO_2 ($m/z = 44$) were recorded. In H_2 temperature-programmed reduction (TPR) of the sample, 0.1 g sample was pretreated at 30 °C in N_2 for 1 h prior to the TPR run. The reduction gas of 10% H_2/N_2 (30 mL min^{-1}) was used and the temperature was heated at 10 °C min^{-1} from RT to 550 °C, and the uptake amounts of H_2 were measured by a thermal conductivity detector (TCD).

3. Results and discussions

3.1. Effect of Cu and Pd loadings on the catalytic activity

The effects of Cu and Pd loadings on the catalytic activity of Pd–Cu–Cl_x/CNT were investigated for CO oxidation and the results are shown in Fig. 1. For the single component catalysts 3.3 wt% Pd/CNT and 6.6 wt% Cu/CNT, their catalytic activities are very poor for low temperature CO oxidation (Fig. 1B): the CO conversion over 6.6 wt% Cu/CNT is only ~1.2% in the temperature range of −40 to 40 °C, and the activity of the 3.3 wt% Pd/CNT catalyst increased with the reaction temperature and its CO conversion at 40 °C was only ~33%.

As shown in Fig. 1A, the activity of Pd–Cu–Cl_x/CNT with a fixed Pd loading (1.7 wt%) for CO oxidation was enhanced gradually with the increase in the Cu amount. When the Cu content reached 6.6–9.9 wt%, the catalytic activity of the catalyst reached the highest, *i.e.*, when the Cu amount was larger than 6.6 wt%, its catalytic activity was hardly changed. Fig. 1B showed the variation in the catalytic activity of Pd–Cu–Cl_x/CNT for CO oxidation with the Pd loading. When the Cu loading (6.6 wt%) was fixed, the catalytic activity of the catalyst always increased with the Pd loading. Moreover, we can find that the increase rate of the catalytic activity became slower when the Pd loading exceeded 3.3 wt%. Taking into account the cost of the catalyst, the loadings of Pd and Cu are chosen to be 3.3 wt% and 6.6 wt%, respectively.

The effect of the calcination temperature of Cu–Cl_x/CNT on the catalytic activity of Pd–Cu–Cl_x/CNT for CO oxidation was investigated and the results are shown in Fig. S2,† in which 1.7 wt% Pd–3.3 wt% Cu–Cl_x/CNT was used as the model catalyst. The results show that the catalytic activity of the catalyst that calcined at 200 °C is slightly higher than the catalyst that calcined at 180 °C or 220 °C.

The carbon support (the commercial wood based (WAC) and coal based (CAC) activated carbon) on the performance of the supported 3.3 wt% Pd–6.6 wt% Cu catalyst was tested and the results are shown in Fig. 2. The results show that the carbon

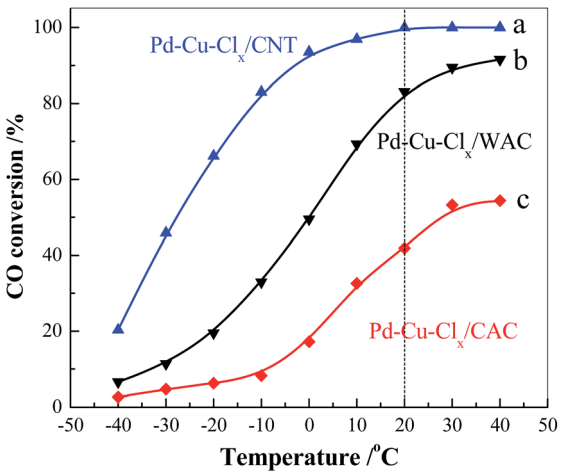

Fig. 2 Catalytic activities of 3.3 wt% Pd–6.6 wt% Cu supported on (a) CNT, (b) WAC, and (c) CAC for CO oxidation (1500 ppm CO and ~3.1% moisture in flow, WHSV of 15 000 mL g^{-1} h^{-1}).

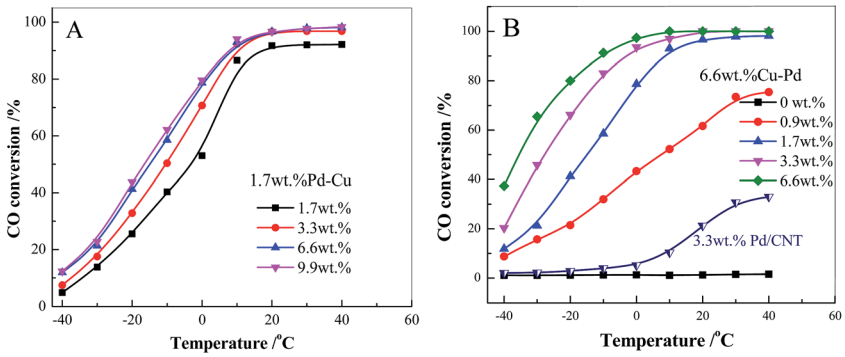

Fig. 1 Effects of (A) Cu and (B) Pd loadings on the activity of Pd–Cu–Cl_x/CNT for CO oxidation (1500 ppm CO and ~3.1% moisture in flow, WHSV of 15 000 mL g^{-1} h^{-1}).

support has an obvious influence on the catalytic activity of supported 3.3 wt% Pd–6.6 wt% Cu catalyst and the catalyst supported on CNT shows a much higher activity than the catalysts on WAC and CAC. At 20 °C, the CO conversion over the 3.3 wt% Pd–6.6 wt% Cu/CNT catalyst reached 100%, and the CO conversions over the 3.3 wt% Pd–6.6 wt% Cu/WAC and 3.3 wt% Pd–6.6 wt% Cu/CAC catalysts are only 83% and 42%, respectively.

3.2. Effects of CO and moisture concentrations in feed gas and WHSV on the catalytic activity

The influence of CO concentration on the CO oxidation over the 3.3 wt% Pd–6.6 wt% Cu/CNT catalyst was investigated and the results are shown in Fig. 3A. The results show that with the increase in the CO concentration, the CO conversion decreased and the temperature (T_{100}) of its complete conversion shifted to a higher temperature, in other words, the catalytic activity decreased. When the concentration of CO in the reactant gas was 750 ppm, T_{100} was 10 °C; when the CO concentration was increased to 1500, 3000 and 5000 ppm, T_{100} increased to 20 °C, 30 °C and 40 °C, respectively. It is suspected that the excess CO_2 produced from the CO oxidation cannot desorb completely in time from the catalyst surface when CO concentration was high, which covered the exposed active sites for CO adsorption. The abovementioned results clearly show a negative influence for relatively high CO concentrations on the CO oxidation over the Pd–Cu–Cl_x/CNT catalyst.

Fig. 3B shows that the activity of 3.3 wt% Pd–6.6 wt% Cu/CNT catalyst was influenced by different moistures in the feed gas. In the absence of water, the 3.3 wt% Pd–6.6 wt% Cu/CNT catalyst showed a lower activity for CO oxidation. When the reactant gas contained 0.6–7.3% moisture, the activity of the catalyst would increase obviously, and the CO could be completely converted at 20 °C. As shown in Fig. 3B, with the increase in water concentration the CO conversion was increased significantly at lower temperatures (<20 °C), and the CO conversion was at a maximum when the moisture was 3.1%. Note that the catalytic performance of this catalyst at 20 °C was much lower than that at 0 °C. The reason ought to be that the CNT support in the catalyst would inevitably absorb some moisture due to having contact with the air before being used. With an increase in the reaction temperature (>0 °C), a part of the adsorbed water would be desorbed and carried away by the feed gas. Because water plays a critical role in the catalytic cycle of Wacker-type catalysts[36] and water adsorbed was desorbed at higher temperatures (as 20 °C), the catalytic performance measured at 20 °C was much lower than that measured at 0 °C. To verify the discussion above, after being pretreated at 120 °C in N_2 for 1 h, the catalytic activity of the 3.3 wt% Pd–6.6 wt% Cu/CNT catalyst was tested under an anhydrous condition, and the results (Fig. S3b†) showed that it exhibited hardly any catalytic activity for CO oxidation.

The effect of the space velocity (WHSV) on the CO conversion over 3.3 wt% Pd–6.6 wt% Cu/CNT was tested, and the results are shown in Fig. 3C. When a WHSV was below 15 000 mL g^{-1} h^{-1}, the CO conversion was hardly influenced by the space velocity. When the WHSV was larger than 15 000 mL g^{-1} h^{-1}, the CO conversion decreased with respect to an increase of space velocity, because the residence time of CO in the catalyst bed decreased due to the speed increase. Therefore, suitably increasing the reaction temperature is needed to achieve

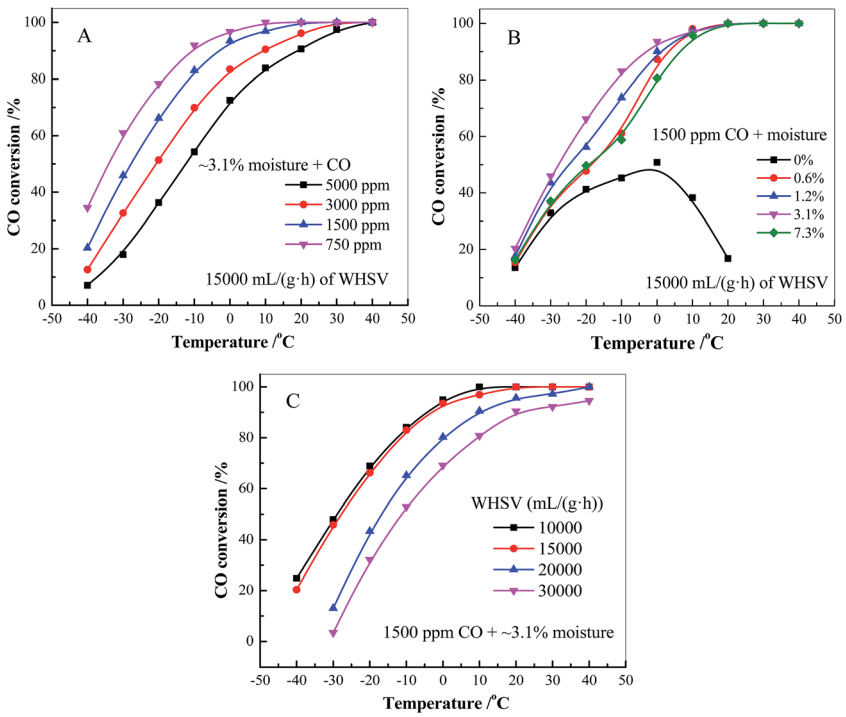

Fig. 3 Effects of (A) CO and (B) moisture concentrations, and (C) WHSV on the CO conversion over the 3.3 wt% Pd–6.6 wt% Cu/CNT catalyst.

a sufficient conversion of CO at a higher space velocity. The results in Fig. 3C show that the decrease of WHSV cannot obviously improve the catalytic performance of the 3.3 wt% Pd–6.6 wt% Cu/CNT catalyst for low temperature CO oxidation when the WHSV is below 15 000 mL g^{-1} h^{-1}.

3.3. The stability of the 3.3 wt% Pd–6.6 wt% Cu/CNT catalyst

Fig. 4A shows the relationship between the CO conversion and the reaction time over 3.3 wt% Pd–6.6 wt% Cu/CNT catalysts for CO oxidation. It can be observed that the 3.3 wt% Pd–6.6 wt% Cu/CNT catalyst exhibited a good stability for CO oxidation at room temperature, and the CO conversion was still retained at around 93% after 60 h of the reaction at 25 °C in the reactant gas, including 3.1% moisture. When the Pd–Cu–Cl_x/Al_2O_3 catalysts prepared by a similar preparation method, the CO conversion was reduced rapidly after 30 h of the reaction at 25 °C with ~3.1% moisture in flow,[25] which shows that the Pd–Cu–Cl_x/Al_2O_3 catalyst has been deactivated.

As shown in Fig. 4, the moisture concentration has an obvious influence on the stability of the catalyst. In the presence of ~0.6% moisture, the initial activity of the catalyst is above 96% CO conversion, and after 1.5 h of the reaction, its CO conversion sharply decreased to 44%. Once the moisture concentration was increased to ~3.1%, the CO conversion could be recovered quickly (Fig. 4B), which shows that relatively high concentration of moisture can improve the catalytic performance of the Pd–Cu–Cl_x/CNT catalyst for CO oxidation. When the water content was increased to ~1.2%, the catalyst showed a slightly better stability and its activity could be unchanged for 3 h, upon which it decreased from 95% to 64% after 21 h of the reaction. In the presence of ~2.1% moisture, the activity of the catalyst can maintain above a 95% CO conversion rate for 16 h, and then gradually decreases to 71% after 44 h of the reaction. When the water content was further increased to ~7.3%, the activity of the catalyst can remain at above 93% of CO conversion for 6 h and then the CO conversion gradually decreases to 73% after 16 h of the reaction, in which a large amount of water becomes condensed on the support surface, resulting in the sharp fall in its activity.

The above results show that the presence of a moderate amount of water is necessary for sustaining the high activity of the 3.3 wt% Pd–6.6 wt% Cu/CNT catalyst. Choi *et al.* thought that the role of H_2O in CO oxidation over supported $PdCl_2$–$CuCl_2$ catalyst is two-fold:[37] water vapor directly takes part in the reaction to form CO_2, and the dissolved Pd and Cu species form the thin layer on the support surface, which were the catalytically active sites for CO oxidation. Kuksenko *et al.* thought that in acidic solutions the CO molecule is activated through coordination in Pd(II) or Cu(I) complexes to produce mixed ligand carbonyls.[38] The Pd–Cu–Cl_x/CNT catalysts were prepared in the HCl solution and the chloride remained on the surface and therefore the adsorbed water layer could be considered to be acidic, similar to the situation described by Kuksenko *et al.*

However, the excessive water vapor in feed gas would impede the activity and stability of the catalyst. This is because at high concentrations, the water vapor would adsorb and condense on the surface of the catalyst, resulting in the aggregation and migration of Cu species into the internal pores. The excess amount of water would decrease the interaction between the Pd and Cu species and decrease the properties of Pd^0 oxidized to Pd^{2+}. The redox cycling would be inhibited, and consequently it would make reduction its main catalytic activity.[39]

3.4. Catalyst characterization

3.4.1. FT-IR spectra of $Cu_2Cl(OH)_3$/CNT. To prove that the $Cu_2Cl(OH)_3$ phase on CNT was pre-synthesized successfully, the *in situ* FT-IR spectra of pre-synthesized $Cu_2Cl(OH)_3$/CNT samples were obtained and are shown in Fig. 5. The results show that, unlike the CNT support (Fig. 5b), the $Cu_2Cl(OH)_3$/CNT samples have two absorption peaks at 3481 and 3400 cm^{-1}, which should be attributed to the hydroxyl stretching modes $\nu(O_1–H_1)/\nu(O_{2/3}–H_{2/3})$ of the $Cu_2Cl(OH)_3$,[25,40] and these two absorption peaks would not disappear after the sample was dried at 120 °C/N_2 for 2 h. The absorption peak intensities at 3481 and 3400 cm^{-1} are weaker when the content of Cu is 9.9 wt% (Fig. 5d), but the intensities of these two absorption peaks would gradually increase with the increase in the Cu loading. These results show that $Cu_2Cl(OH)_3$ has existed on CNT after the impregnation and calcination at 200 °C.

3.4.2. ICP-OES and N_2 physisorption. The compositions of Pd and Cu in the catalysts were measured by ICP-OES method and the data is listed in Table 1. The results show that the Pd

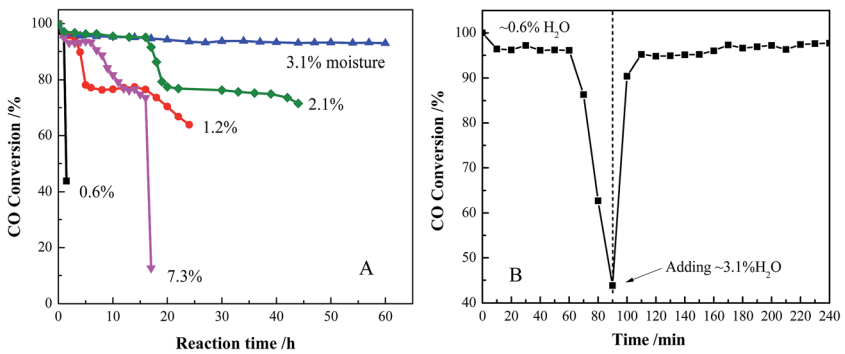

Fig. 4 Catalytic stability of the 3.3 wt% Pd–6.6 wt% Cu/CNT catalyst for CO oxidation with different moisture concentrations at 25 °C (1500 ppm CO, WHSV of 15 000 mL g^{-1} h^{-1}).

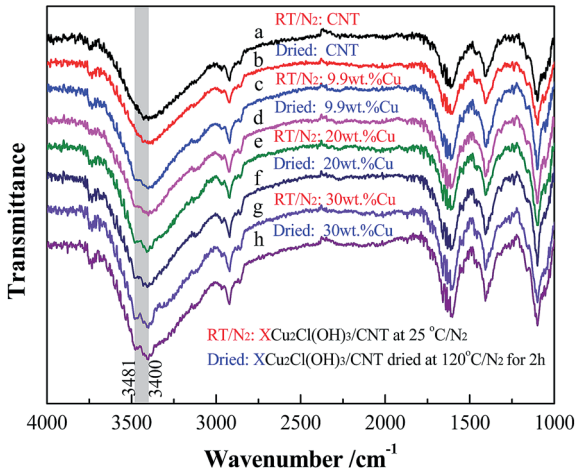

Fig. 5 *In situ* FT-IR spectra of (a and b) CNT, and $Cu_2Cl(OH)_3$/CNT with (c and d) 9.9 wt% Cu, (e and f) 20 wt% Cu and (g and h) 30 wt% Cu; and (a, c, e and g) at 25 °C/N_2 and (b, d, f and g) after 2 h of drying at 120 °C/N_2.

and Cu contents in all the samples are close to the theoretical value in the synthesis solution, which proves that the Pd and Cu species can be perfectly supported on the CNT surface by the two-step impregnation method. Table 1 also shows the textural properties of the CNT support and Pd–Cu–Cl_x/CNT catalysts. We can observe that the BET surface area of the catalyst is decreased with an increase in the loadings of Pd and Cu. The average pore diameter and pore volume of the CNT carrier are 22.1 nm and 1.554 $cm^3\ g^{-1}$, respectively. Its average pore diameter becomes larger and the pore volume becomes smaller after introducing of Pd and Cu, which indicates that the Pd and Cu species have partially blocked some minor pores of the CNT carrier.

3.4.3. XRD. The XRD patterns of Pd–Cu–Cl_x/CNT catalysts are shown in Fig. 6. The diffraction peaks of Pd species cannot be observed in all the catalysts, indicating that the Pd species were highly dispersed on the surface of CNT support or below the detection limit of XRD. Moreover, the four main diffraction peaks at $2\theta = 16.19°$, 30.95°, 39.75° and 50.46° are ascribed to the phase of chinoatacamite $Cu_2Cl(OH)_3$ (JCPDS 50-1559). The results in Fig. 6A show that the peak intensity of $Cu_2Cl(OH)_3$ is increased with the increase in the Cu loading, when the Pd loading is fixed at 1.7 wt%. When the Cu loading maintains at 6.6 wt% in the catalyst, the diffraction peaks of $Cu_2Cl(OH)_3$ are hardly changed with the increase in the Pd content (Fig. 6B). It clearly indicates that the crystallinity of $Cu_2Cl(OH)_3$ phase is relevant with the Cu loading, *i.e.*, the higher the Cu loading, the better the crystallinity of $Cu_2Cl(OH)_3$ is obtained. Park *et al.*[41] demonstrated that $Cu_2Cl(OH)_3$ was regarded as the active copper phase of Wacker-type catalysts. Thus, when the Pd loading was fixed, the stronger intensity of $Cu_2Cl(OH)_3$

Table 1 Physicochemical properties of CNT carrier and Pd–Cu–Cl_x/CNT catalysts

Sample (on CNT)	Pd content[a] (wt%)	Cu content[a] (wt%)	BET surface area ($m^2\ g^{-1}$)	Average pore diameter (nm)	Pore volume ($cm^3\ g^{-1}$)
CNT	—	—	263	22.1	1.554
1.7 wt% Pd–1.7 wt% Cu	1.7	1.6	212	28.7	1.516
1.7 wt% Pd–3.3 wt% Cu	1.7	3.1	202	30.7	1.549
1.7 wt% Pd–6.6 wt% Cu	1.7	6.1	192	27.9	1.337
1.7 wt% Pd–9.9 wt% Cu	1.7	9.2	183	26.9	1.227
0.9 wt% Pd–6.6 wt% Cu	0.9	6.1	193	26.9	1.353
3.3 wt% Pd–6.6 wt% Cu	3.1	6.2	184	25.6	1.178
6.6 wt% Pd–6.6 wt% Cu	6.4	6.2	168	26.2	1.098

[a] Determined by ICP-OES.

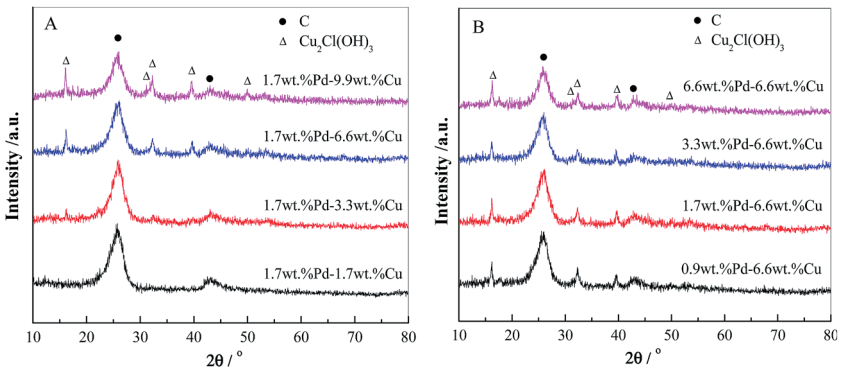

Fig. 6 XRD Patterns of the Pd–Cu–Cl_x/CNT catalysts with different (A) Cu loadings and (B) Pd loadings.

diffraction peaks, the higher its catalytic activity would be, which is consistent with our experimental results.

3.4.4. TEM. Fig. 7 shows the TEM images of CNT and 3.3 wt% Pd–6.6 wt% Cu/CNT catalyst. In the TEM image of Fig. 7A, the morphology characteristic of carbon nanotubes can be observed clearly. The Pd and Cu species can be perfectly supported on the CNT surface by the two-step impregnation method, and the catalyst particles (about 10–15 nm) are distributed uniformly on the outside surface of the CNT support.

3.4.5. H_2-TPR. The TPR profiles of 3.3 wt% Pd/CNT, 6.6 wt% Cu/CNT and Pd–Cu–Cl_x/CNT are shown in Fig. 8, and the H_2 consumption amounts in the TPR profiles are listed in Table 2. As shown in Fig. 8B, 3.3 wt% Pd/CNT exhibits a reduction peak at 145 °C and 6.6 wt% Cu/CNT has two reduction peaks at 275 °C and 410 °C, respectively, in which the former is ascribed to the reduction of Cu^{2+} to Cu^{+}, and the latter is caused by the reduction of Cu^{+} to Cu^{0}. In the TPR profiles of Pd–Cu–Cl_x/CNT catalysts, there are two reduction peaks, the sharp α peak is ascribed to the co-reduction of Pd and Cu species due to the strong interaction between the Pd and Cu species, and the β peak is assigned to the reduction of copper species that did not interact with the palladium species.[30,39]

As shown in Fig. 8A, with the increase of the Cu loading in the Cu–1.7 wt% Pd/CNT catalysts, the H_2 consumption in the α peak increased significantly (from 322 to 1019 μmol g^{-1}) and the peak shifted slightly towards a higher temperature (from 197 to 220 °C), and the H_2 consumption in the β peak increased smoothly as well (from 26 to 515 μmol g^{-1}). However, when the Cu loading increased from 6.6 wt% to 9.9 wt%, the β peak area increased significantly from 363 to 515 μmol g^{-1}, which indicates that the excess amount of Cu could not interact with Pd species. As shown in Fig. 8B, when the Pd loading is increased in the 6.6 wt% Cu–Pd/CNT catalyst, the H_2 consumption of β peak of Cu reduction decreased from 370 to 165 μmol g^{-1} gradually, due to the more Pd species interacting with the Cu species. Moreover, the α peak of the co-reduction of Pd and Cu species became stronger, *i.e.*, consuming more H_2 (from 646 to 1114 μmol g^{-1}) and shifted towards the lower temperature (from 230 to 175 °C), which indicated that the existence of Pd species facilitate the reduction of Cu^{2+} ions.

Compared with 3.3 wt% Pd/CNT, the reduction temperature of 6.6 wt% Cu/CNT is much higher, showing that the Pd species is much more easily reduced than the Cu species. For the 3.3 wt% Pd–6.6 wt% Cu/CNT catalyst, the temperatures of its reduction peaks are higher than that of Pd species and lower than that of Cu species. Its H_2 consumption amounts of α peak and β peak are 1017 and 170 μmol g^{-1}, respectively, and their sum (1187 μmol g^{-1}) approaches the theoretical H_2 consumption (1230 μmol g^{-1}) in the reduction of both Pd and Cu species. Note that the H_2 consumption of α peak is more than that of Pd (291 μmol g^{-1}) or Cu (969 μmol g^{-1}) species, thus it can be said that the α peak comes from the co-reduction of Pd and Cu species.

These abovementioned results show that the Pd species is much more easily reduced than the Cu species, the presence of Pd promotes the Cu reduction and that the presence of Cu decreases the Pd reduction by their interaction, and the proper

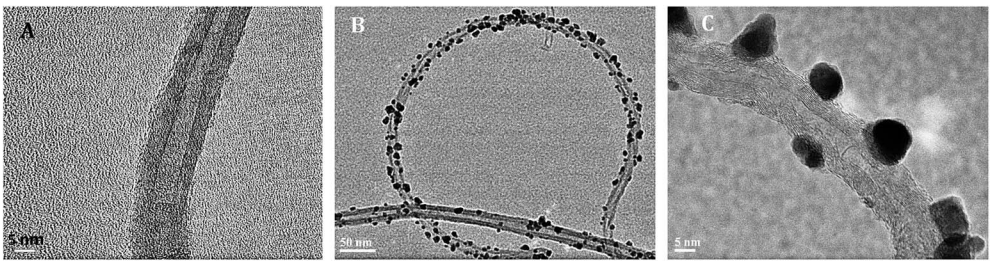

Fig. 7 TEM images of (A) CNT and (B and C) 3.3 wt% Pd–6.6 wt% Cu/CNT catalyst.

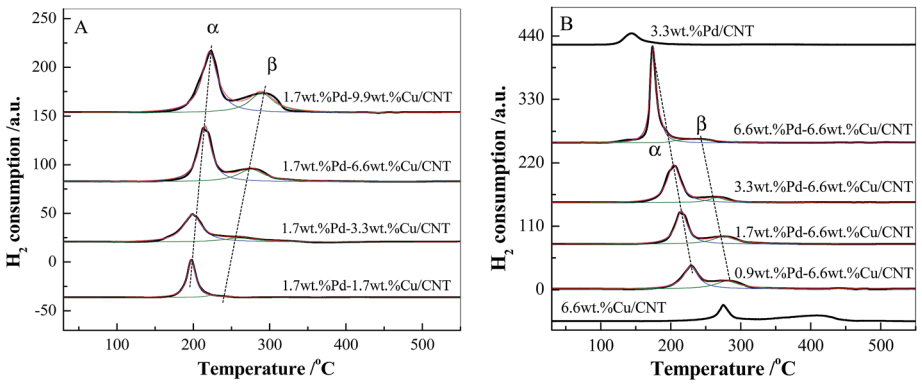

Fig. 8 TPR profiles of the Pd–Cu–Cl_x/CNT catalysts with different (A) Cu loadings and (B) Pd loadings.

Table 2 H_2 consumption amounts in TPR profiles of the Pd–Cu–Cl_x/CNT catalysts

Sample (on CNT)	H_2 uptake (μmol g^{-1})/ top temp. (°C)		Theoretical H_2 uptake[a] (μmol g^{-1})	
	α peak	β peak	Pd	Cu
1.7 wt% Pd–1.7 wt% Cu	322/197	26/225	160	250
1.7 wt% Pd–3.3 wt% Cu	542/200	142/260	160	484
1.7 wt% Pd–6.6 wt% Cu	761/215	363/275	160	953
1.7 wt% Pd–9.9 wt% Cu	1019/220	515/290	160	1422
0.9 wt% Pd–6.6 wt% Cu	646/230	370/280	85	953
3.3 wt% Pd–6.6 wt% Cu	1017/205	170/265	291	969
6.6 wt% Pd–6.6 wt% Cu	1114/175	165/232	602	969

[a] Calculated by actual Pd and Cu loadings obtained by ICP-OES.

loadings of Pd and Cu can reach the moderate interaction between Cu and Pd, which is favorable for the improvement of its catalytic performance for CO oxidation.

3.4.6. CO-TPD. The TPD-MS profiles for CO and CO_2 after CO adsorbed on the catalyst are shown in Fig. 9. It can be observed that all the samples showed one peak of CO and CO_2 desorption at 125–140 °C. For the CO desorption (Fig. 9A and B), the peak area increased significantly with the increase in the Pd loading than the Cu loading on the CNT carrier, *i.e.*, increasing the Pd amount can significantly improve the CO adsorption than increasing the Cu amount, and compared with Cu species, Pd is a more effective site for the CO adsorption. This is because, in the catalytic oxidation of CO, the Pd species are the main active sites for CO and the Cu species are the active sites for oxygen,[42] and the increase of Pd loading can enhance the number of active sites on the catalyst for CO adsorption.

In the CO_2 desorption curves (Fig. 9C and D), with the increase of Pd or Cu loading, the peak area of CO_2 desorption also increased, which indicates that the adsorbed CO can react with the oxygen-containing functional groups on the surface of CNT immediately,[43,44] and the amount of desorbed CO_2 increased with the increase in CO adsorption sites and active oxygen sites. Therefore, the low-temperature peaks of CO and CO_2 desorption is closely related with the activity of the catalyst for CO oxidation,[45] and CO desorbed at low temperature plays a crucial role in the low-temperature CO oxidation.[46]

3.4.7. XPS. The Pd–Cu–Cl_x/CNT catalysts were tested by XPS, the Cu $2p_{3/2}$ and Pd 3d XPS spectra are shown in Fig. 10 and S4,† respectively, and the surface compositions of Pd and Cu species obtained based on the XPS data are summarized in Table 3.

By fitting the Pd 3d XPS spectra of all the catalysts, only the Pd^{2+} peak could be found (337.8 and 343.1 eV) in their spectra (Fig. S4†). In the Cu 2p XPS spectra of all the catalysts, there are the Cu^{+} (932.6 eV) and Cu^{2+} (934.4 eV) species (Fig. 10). The amounts of Pd^{2+} and Cu^{2+} on the catalyst surface increase with the increase in the Pd and Cu loadings. As shown in Table 3, in the 1.7 wt% Pd–Cu–Cl_x/CNT catalyst, with the increase in the Cu loading from 1.7 to 9.9 wt%, the surface Cu^{2+} species increased

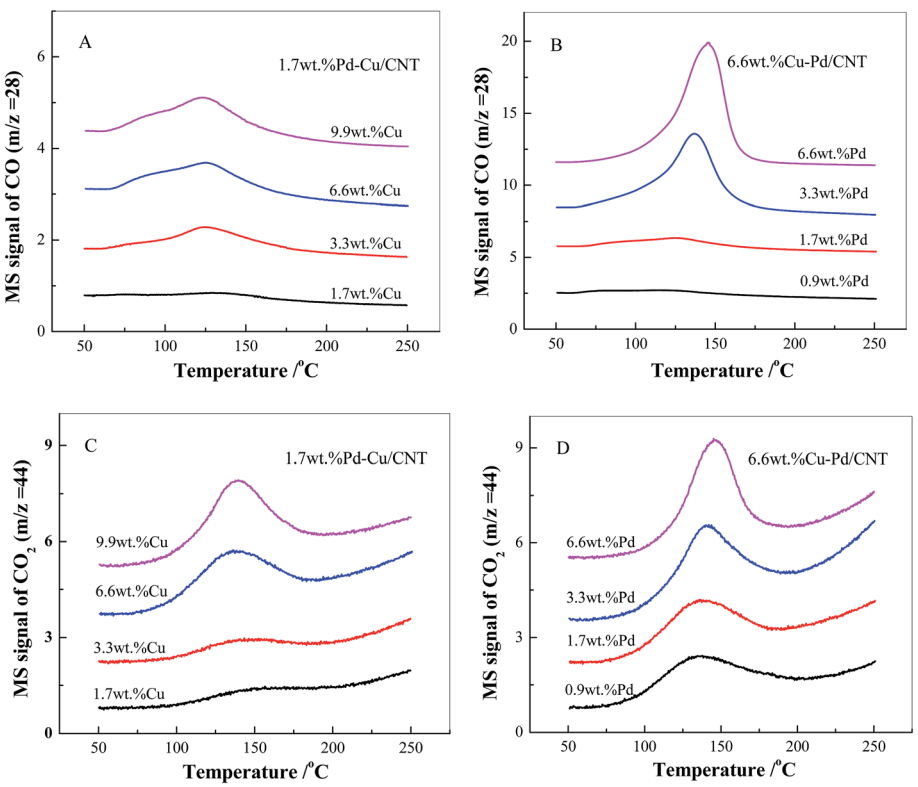

Fig. 9 TPD profiles of CO ($m/z = 28$) and CO_2 ($m/z = 44$) over Pd–Cu–Cl_x/CNT catalysts with different (A and C) Cu and (B and D) Pd loadings.

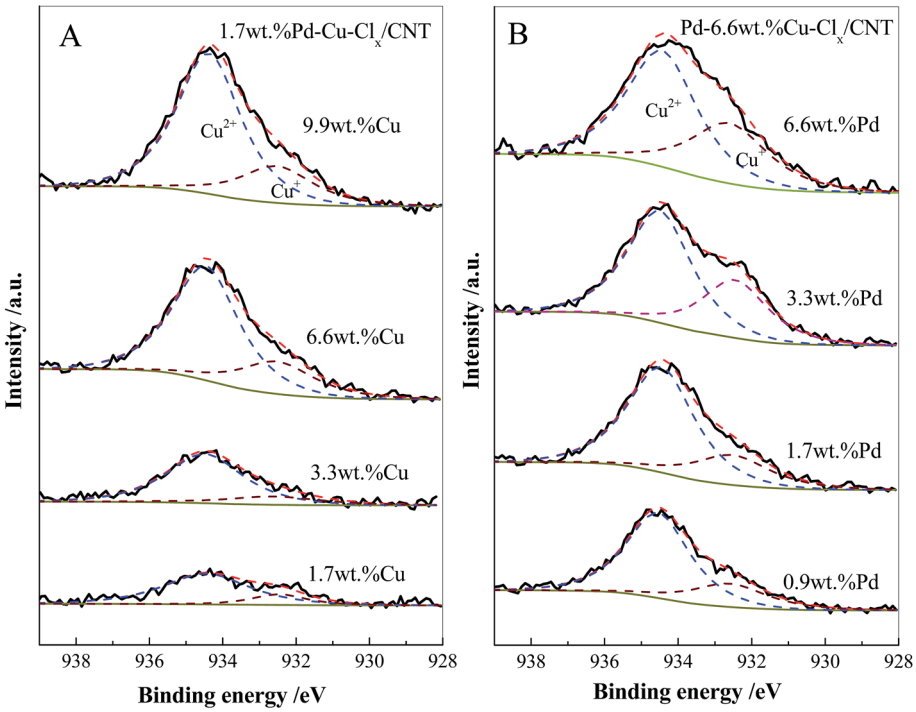

Fig. 10 Cu $2p_{3/2}$ XPS spectra of (A) 1.7 wt% Pd–Cu/CNT and (B) 6.6 wt% Cu–Pd/CNT catalysts.

Table 3 Surface composition of the Pd–Cu–Cl$_x$/CNT catalysts calculated based on the XPS data

Sample (on CNT)	Pd^{2+} (atom%)	Cu^{2+} (atom%)	Cu^{+} (atom%)	Total Cu (atom%)
1.7 wt% Pd–1.7 wt% Cu	0.21	0.40	0.18	0.58
1.7 wt% Pd–3.3 wt% Cu	0.22	0.59	0.17	0.76
1.7 wt% Pd–6.6 wt% Cu	0.25	1.16	0.26	1.42
1.7 wt% Pd–9.9 wt% Cu	0.27	1.42	0.31	1.73
0.9 wt% Pd–6.6 wt% Cu	0.12	1.06	0.22	1.28
3.3 wt% Pd–6.6 wt% Cu	0.39	1.30	0.47	1.77
6.6 wt% Pd–6.6 wt% Cu	0.62	1.33	0.76	2.09

from 0.4 to 1.42 wt% and the surface Cu^{+} species increased from 0.18 to 0.31 wt%, whereas the surface Pd^{2+} species also increased from 0.21 to 0.27 wt%. For the Pd–6.6 wt% Cu–Cl$_x$/CNT catalyst, with an increase in the Pd loading from 0.9 to 6.6 wt%, the surface of Pd^{2+} species increased from 0.12 to 0.62 wt%, whereas the Cu^{2+} + Cu^{+} species increased from 1.28 to 2.09 wt%, in which the Cu^{+} species increased from 0.22 to 0.76 wt%.

3.5. Discussion about the catalytic oxidation mechanism of CO

Many researchers thought that the catalytic mechanism of CO oxidation on the supported $PdCl_2$–$CuCl_2$ catalyst is similar to the well-known Wacker process, which is viewed as a co-catalysis process.

$$CO + PdCl_2 + H_2O \rightarrow CO_2 + Pd(0) + 2HCl$$

$$Pd(0) + 2CuCl_2 \rightarrow PdCl_2 + 2CuCl$$

$$2CuCl + 2HCl + \tfrac{1}{2}O_2 \rightarrow 2CuCl_2 + H_2O$$

In the catalytic oxidation of CO over the supported Wacker catalyst, Pd species are the main active sites for CO and Cu species are the active sites for O_2, and a moderate amount of H_2O is necessary. When $PdCl_2$–$CuCl_2$ is supported on Al_2O_3, the presence of excess H_2O would cause the formation of a poisonous species, because H_2O is easily dissociated to absorb –H and –OH species that can occupy the surface active sites of Pd and Cu.[42] The rate-determining step is the transformation of CO–Pd–OH to Pd–COOH and its energy barrier is only 0.52 eV, indicating that CO oxidation occurs very easily over Pd–Cu–Cl$_x$/γ-Al_2O_3.[42] In the catalytic cycle, the Cu^{2+} species plays an important role in the process of oxidizing Pd^0 to Pd^{2+} (or Pd^{+}). Moreover, the solid copper phase of $Cu_2Cl(OH)_3$ pre-synthesized on the carbon support showed better reactivity than $CuCl_2 \cdot H_2O$ for oxidizing the Pd^0 species.[47]

Associated with the catalytic activities in Fig. 1, we can find that the catalytic activity of 1.7 wt% Pd–Cu–Cl$_x$/CNT catalyst increased slowly with an increase in the amount of surface Cu^{2+} species accompanied by an increase of surface Pd^{2+} species. For the Pd–6.6 wt% Cu–Cl$_x$/CNT catalyst, its activity increased substantially with an increase in the amount of surface Pd^{2+} species and surface Cu^{+} species. This situation shows that active adsorption of CO needs more Pd^{2+} species, and increasing the amount of surface Cu^{+} species causes the active adsorption of the oxygen on the Cu species or the process of oxidizing Pd^0 to Pd^{2+} (or Pd^{+}) easier.

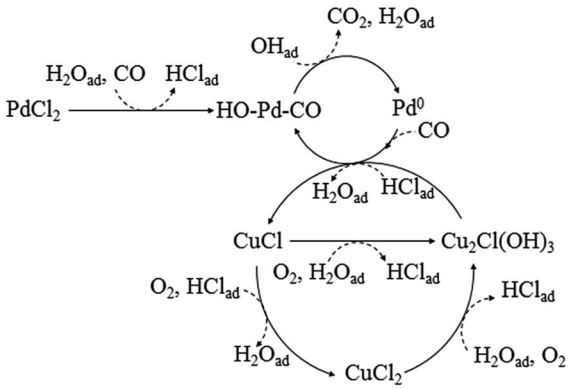

Fig. 11 Proposed catalytic oxidation pathways of CO over Pd–Cu–Cl_x/CNT catalyst.

Based on the results here and reported,[28,36,37,42,47] the mechanism of CO oxidation over the Pd–Cu–Cl_x/CNT catalysts was proposed as in Fig. 11. In this catalytic cycle, the Pd^{2+} ions are the active sites for CO adsorption and $Cu_2Cl(OH)_3$ is regarded as the active copper phase of Wacker-type catalysts. After CO adsorbed on $PdCl_2$, with the help of adsorbed water, HO–Pd–CO formed. The transformation of CO–Pd–OH to Pd–COOH is the rate-determining step, and Pd–COOH intermediate directly dissociates –H to form Pd–CO_2, then releases CO_2 to the gas phase and produces Pd^0.[42] Pd^0 then adsorbs CO to form PdCO. PdCO attacks the hydroxyl of $CuCl(OH)_3$ to form HO–Pd–CO and CuCl species by the help of the adsorbed HCl. Subsequently, CuCl is re-oxidized by O_2 to form $Cu_2Cl(OH)_3$ with the help of the adsorbed water and HCl molecules. The $Cu_2Cl(OH)_3$ species shows better reactivity than the $CuCl_2 \cdot H_2O$ for oxidizing the Pd^0 species,[47] thus the catalytic cycle is complete. As shown in Fig. 11, adsorbed H_2O plays a very important role in whole catalytic cycle. Because CNT is the multi-wall nanotubes (Fig. 7A) and different from alumina and activated carbon (AC), the Pd–Cu–Cl_x was supported on the external surface of CNT (Fig. 7C), and water would adsorb and condense inside the CNT tube. For this $PdCl_2$–$CuCl_2$/CNT catalyst system, its water content must be more than that in the catalysts supported on alumina or AC. Therefore, an optimum water vapor concentration is different for different supported Wacker catalysts.

4. Conclusions

In summary, the Pd–Cu–Cl_x/CNT catalysts were prepared by the two-step impregnation method, and exhibited the higher catalytic performance for CO oxidation than that supported on activated carbon. With the increase in the Pd and Cu loadings, its catalytic activity increased. The presence of a moderate amount of water is necessary for sustaining the high activity of the Pd–Cu–Cl_x/CNT catalyst, but excessive water vapor in the feed gas would hinder the activity and stability of the catalyst. When the moisture was 3.1% in the reactant gas, the CO conversion was still retained at around 93% after 60 h of the reaction at 25 °C over the 3.3 wt% Pd–6.6 wt% Cu/CNT catalyst, which shows that this catalyst has a very good stability and water-resistance at room temperature.

In the 3.3 wt% Pd–6.6 wt% Cu/CNT catalyst, the $Cu_2Cl(OH)_3$ phase on CNT can be measured by the *in situ* FT-IR spectroscopy and XRD, and the formation of the $Cu_2Cl(OH)_3$ species can effectively improve the catalytic activity for CO oxidation. The CO-TPD results show that the CO desorption peak area increased significantly with the increase in the Pd loading compared to the Cu loading on the CNT carrier, which shows that the Pd^{2+} ions are the active sites for CO adsorption, and the amount of desorbed CO_2 increased due to the increase in CO adsorption sites and active oxygen sites. The XPS results showed that the surface Pd^{2+} and Cu^{2+}/Cu^{+} species would increase simultaneously with the increase of the Pd or Cu loading. Moreover, more Pd^{2+} active sites or species present on the catalyst surface is beneficial for CO adsorption, and the increase of the surface active Cu^{2+} species can improve the active adsorption of oxygen on the catalyst and the process of oxidizing the Pd^0 species.

Acknowledgements

This study was financially supported by the National Natural Science Foundation of China (21273150, 21571061), the National Basic Research Program of China (2013CB933201), the national high technology research and development program of China (2015AA034603, 2012AA062703), the Shanghai Natural Science Foundation (12ZR1430800), and the Shanghai Innovation Program (12YZ161).

References

1 X. Yang, L. Yang, S. Lin and R. Zhou, *Chin. J. Catal.*, 2014, **35**, 1267.
2 C. Jones, S. H. Taylor, A. Burrows, M. J. Crudace, C. J. Kiely and G. J. Hutchings, *Chem. Commun.*, 2008, 1707.
3 B. K. Chang and B. J. Tatarchuk, *J. Mater. Eng. Perform.*, 2006, **15**, 453.
4 N. Du, H. Zhang, X. Ma and D. Yang, *Chem. Commun.*, 2008, 6182.
5 L. Li, A. Wang, B. Qiao, J. Lin, Y. Huang, X. Wang and T. Zhang, *J. Catal.*, 2013, **299**, 90.
6 B. Qiao, A. Wang, X. Yang, L. F. Allard, Z. Jiang, Y. Cui, J. Liu, J. Li and T. Zhang, *Nat. Chem.*, 2011, **3**, 634.
7 G. Glaspell, L. Fuoco and M. S. El-Shall, *J. Phys. Chem. B*, 2005, **109**, 17350.
8 Z. W. Wang, B. Li, M. S. Chen, W. Z. Weng and H. L. Wan, *Sci. China: Chem.*, 2010, **53**, 2047.
9 S. T. Daniells, M. Makkee and J. A. Moulijn, *Catal. Lett.*, 2005, **100**, 39.
10 M. Daté, M. Okumura, S. Tsubota and M. Haruta, *Angew. Chem., Int. Ed.*, 2004, **43**, 2129.
11 J. M. C. Soares, M. Hall, M. Cristofolini and M. Bowker, *Catal. Lett.*, 2006, **109**, 103.
12 S. H. Wu, X. C. Zheng, S. R. Wang, D. Z. Han, W. P. Huang and S. M. Zhang, *Catal. Lett.*, 2004, **96**, 49.

13 W. S. Lee, B. Z. Wan, C. N. Kuo, W. C. Lee and S. Cheng, *Chem. Commun.*, 2007, 1604.
14 H. Zhang, D. Lin, G. Xu, J. Zheng, N. Zhang, Y. Li and B. H. Chen, *Int. J. Hydrogen Energy*, 2015, **40**, 1742.
15 E. Y. Ko, E. D. Park, H. C. Lee, D. Lee and S. Kim, *Angew. Chem., Int. Ed.*, 2007, **46**, 734.
16 S. Huang, K. Hara and A. Fukuoka, *Energy Environ. Sci.*, 2009, **2**, 1060.
17 A. Fukuoka, J. Kimura, T. Oshio, Y. Sakamoto and M. Ichikawa, *J. Am. Chem. Soc.*, 2007, **129**, 10120.
18 J. Y. Park, Y. Zhang, M. Grass, T. Zhang and G. A. Somorjai, *Nano Lett.*, 2008, **8**, 673.
19 P. Bera, A. Gayen, M. S. Hegde, N. P. Lalla, L. Spadaro, F. Frusteri and F. Arena, *J. Phys. Chem. B*, 2003, **107**, 6122.
20 W. Song, A. S. Poyraz, Y. Meng, Z. Ren, S. Y. Chen and S. L. Suib, *Chem. Mater.*, 2014, **26**, 4629.
21 M. Krämer, T. Schmidt, K. Stöwe and W. F. Maier, *Appl. Catal., A*, 2006, **302**, 257.
22 D. J. Koh, J. H. Song, S. W. Ha and I. S. Nam, *Korean J. Chem. Eng.*, 1997, **14**, 486.
23 E. D. Park and J. S. Lee, *J. Catal.*, 2000, **193**, 5.
24 Y. Shen, G. Lu, Y. Guo and Y. Wang, *Chem. Commun.*, 2010, **46**, 8433.
25 X. Du, H. Li, J. Yu, X. Xiao, Z. Shi, D. Mao and G. Lu, *Catal. Sci. Technol.*, 2015, **5**, 3970.
26 K. D. Kim, I. S. Nam, J. S. Chung, J. S. Lee, S. G. Ryu and Y. S. Yang, *Appl. Catal., B*, 1994, **5**, 103.
27 I. A. Kotareva, I. V. Oshanina, K. Y. Odintsov, L. G. Bruk and O. N. Tenkin, *Kinet. Catal.*, 2008, **49**, 18.
28 F. Wang, K. Zhao, H. Zhang, Y. Dong, T. Wang and D. He, *Chem. Eng. J.*, 2014, **242**, 10.
29 C. W. Lee, S. J. Park, Y. S. Kim and P. J. Chong, *Bull. Korean Chem. Soc.*, 1995, **16**, 296.
30 L. Wang, Y. Feng, Y. Zhang, Y. Lou, G. Lu and Y. Guo, *Fuel*, 2012, **96**, 440.
31 Y. Wang, L. Fan, R. Wu, J. Shi, X. Li and Y. Zhao, *J. Fuel Chem. Technol.*, 2015, **43**, 1076.
32 Y. Wang, J. Shi, R. Wu, X. Li and Y. Zhao, *Appl. Clay Sci.*, 2016, **119**, 126.
33 Y. M. Dai, T. C. Pan, W. J. Liu and J. M. Jehng, *Appl. Catal., B*, 2011, **103**, 221.
34 D. Zhang, H. Mai, L. Huang and L. Shi, *Appl. Surf. Sci.*, 2010, **256**, 6795.
35 C. H. Kuo, W. Li, W. Song, Z. Luo, A. S. Poyraz, Y. Guo, A. W. K. Ma, S. L. Suib and J. He, *ACS Appl. Mater. Interfaces*, 2014, **6**, 11311.
36 Y. Shen, G. Lu, Y. Guo, Y. Wang, Y. Guo and X. Gong, *Catal. Today*, 2011, **175**, 558.
37 K. I. Choi and M. A. Vannice, *J. Catal.*, 1991, **127**, 489.
38 E. L. Kuksenko, V. A. Golodov and M. T. Abilov, *React. Kinet. Catal. Lett.*, 1989, **38**, 215.
39 Y. Feng, L. Wang, Y. Zhang, Y. Guo, Y. Guo and G. Lu, *Chin. J. Catal.*, 2013, **34**, 923.
40 X. D. Liu, M. Hagihala, X. G. Zheng and Q. X. Guo, *Vib. Spectrosc.*, 2011, **56**, 177.
41 E. D. Park and J. S. Lee, *J. Catal.*, 1998, **180**, 123.
42 C. Shen, H. Li, J. Yu, G. Wu, D. Mao and G. Lu, *ChemCatChem*, 2013, **5**, 2813.
43 V. Datsyuk, M. Kalyva, K. Papagelis, J. Parthenios, D. Tasis, A. Siokou, I. Kallitsis and C. Galiotis, *Carbon*, 2008, **46**, 833.
44 H. Ago, T. Kugler, F. Cacialli, W. R. Salaneck, M. S. P. Shaffer, A. H. Windle and R. H. Friend, *J. Phys. Chem. B*, 1999, **103**, 8116.
45 J. Li, G. Lu, G. Wu, D. Mao, Y. Guo, Y. Wang and Y. Guo, *RSC Adv.*, 2013, **3**, 12409.
46 J. Li, G. Lu, G. Wu, D. Mao, Y. Wang and Y. Guo, *Catal. Sci. Technol.*, 2012, **2**, 1865.
47 E. D. Park, S. H. Choi and J. S. Lee, *J. Phys. Chem. B*, 2000, **104**, 5586.